Impact of the equation of state on the evolution of rapidly rotating core collapse supernovae

AG GdR OG, Lyon

Marco Cusinato
marco.cusinato@cea.fr
Collaborators: Martin Obergaulinger, Miguel Ángel Aloy Torás, Matteo Bugli, Andrea Celati

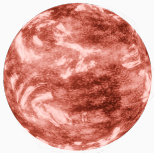
October 5th 2026

Fondos Next Generation en la Comunitat Valenciana

Introduction and numerical setup

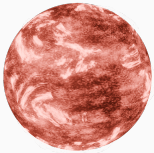
Core Collapse supernovae

- Final stages of the evolution of massive stars;



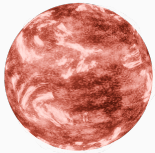
Core Collapse supernovae

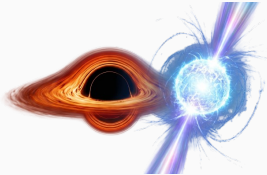
- Final stages of the evolution of massive stars;
- Formation channels of **black holes (BH)** and **neutron stars (NS)**;



CORE COLLAPSE SUPERNOVAE

- Final stages of the evolution of massive stars;
- Formation channels of **black holes (BH)** and **neutron stars (NS)**;
- Multimessenger sources: electromagnetic radiation, **neutrinos**, and **gravitational waves (GWs)**, emitted from the **proto-neutron star (PNS)**.







NUMERICAL SETUP

- Five full-3D simulations;



NUMERICAL SETUP

- Five full-3D simulations;
- **Code**: `Aenus-ALCAR` (Obergaulinger 2008);



NUMERICAL SETUP

- Five full-3D simulations;
- **Code**: `Aenus-ALCAR` (Obergaulinger 2008);
- **Numerics**: Special-relativistic magneto-hydrodynamics (SRMHD) coupled with energy dependent two-moment scheme (M1) with three species ν_e, $\bar{\nu}_e$, $\nu_x = (\nu_\mu, \bar{\nu}_\mu, \nu_\tau, \bar{\nu}_\tau)$;



NUMERICAL SETUP

- Five full-3D simulations;
- **Code**: `Aenus-ALCAR` (Obergaulinger 2008);
- **Numerics**: Special-relativistic magneto-hydrodynamics (SRMHD) coupled with energy dependent two-moment scheme (M1) with three species ν_e, $\bar{\nu}_e$, $\nu_x = (\nu_\mu, \bar{\nu}_\mu, \nu_\tau, \bar{\nu}_\tau)$;
- **Grid**: $r \in [0, 10^{10}]$cm (lin/log-spaced, $n_r = 340/240$), $\theta \in [0, \pi]$ (n_θ=64), $\phi \in [0, 2\pi]$ (n_ϕ=128), $E_\nu \in [0, 340]$MeV ($n_\nu = 10$);



NUMERICAL SETUP

- Five full-3D simulations;
- **Code**: `Aenus-ALCAR` (Obergaulinger 2008);
- **Numerics**: Special-relativistic magneto-hydrodynamics (SRMHD) coupled with energy dependent two-moment scheme (M1) with three species ν_e, $\bar{\nu}_e$, $\nu_x = (\nu_\mu, \bar{\nu}_\mu, \nu_\tau, \bar{\nu}_\tau)$;
- **Grid**: $r \in [0, 10^{10}]\mathrm{cm}$ (lin/log-spaced, $n_r = 340/240$), $\theta \in [0, \pi]$ (n_θ=64), $\phi \in [0, 2\pi]$ (n_ϕ=128), $E_\nu \in [0, 340]\mathrm{MeV}$ ($n_\nu = 10$);
- **Model**: $35\,\mathrm{M}_\odot$ Wolf-Rayet star (Heger *et al.* 2006).



Model and EOS selection

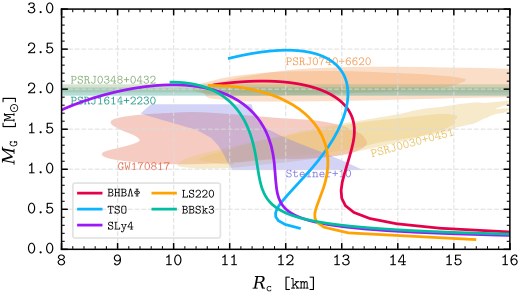
- Original initial **fast rotation** profile ($\approx 2\,\mathrm{rad/s}$);

Model and EOS selection

- Original initial **fast rotation** profile ($\approx 2\,\mathrm{rad/s}$);
- Original **magnetic field** replaced with **weak** dipolar field ($B_{\mathrm{pol}} = B_{\mathrm{tor}} = 10^6\,\mathrm{G}$);

MODEL AND EOS SELECTION

- Original initial **fast rotation** profile ($\approx 2\,\mathrm{rad/s}$));
- Original **magnetic field** replaced with **weak** dipolar field ($B_{\mathrm{pol}} = B_{\mathrm{tor}} = 10^6\,\mathrm{G}$);
- Five nuclear EOSs: **BHB$\Lambda\phi$**, **BBSk3**, **LS220**, **SLy4**, and **TSO**, compatible with astrophysical constraints.

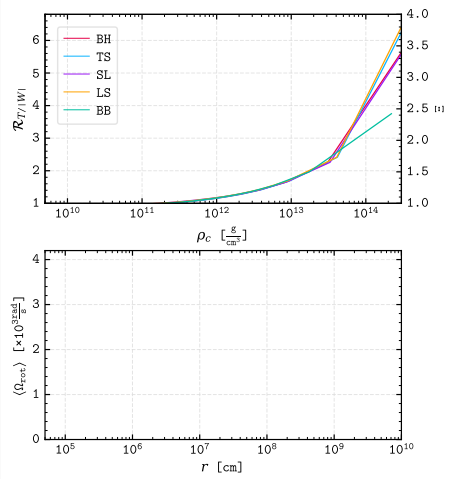


Results

COLLAPSE EVOLUTION

- Normalised rotational parameter of the inner core

$$\mathcal{R}_{T/|W|}(\rho_c) = \frac{T/|W|(\rho_c)}{T/|W|(t=0)};$$



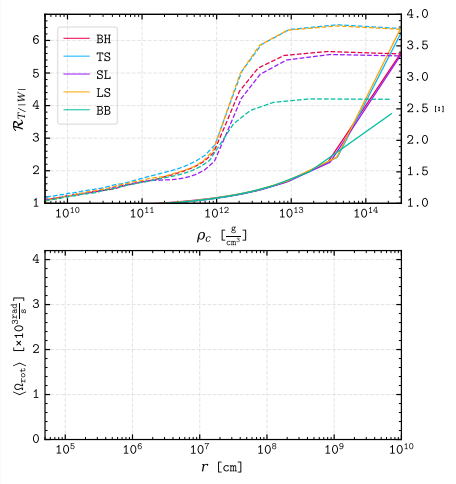
COLLAPSE EVOLUTION

- Normalised rotational parameter of the inner core

$$\mathcal{R}_{T/|W|}(\rho_c) = \frac{T/|W|(\rho_c)}{T/|W|(t=0)};$$

- Homology deviation parameter of the inner core

$$\Xi(\rho_c) = \frac{T/|W|(\rho_c)}{T/|W|(t=0)} \frac{R(\rho_c)}{R(t=0)};$$



COLLAPSE EVOLUTION

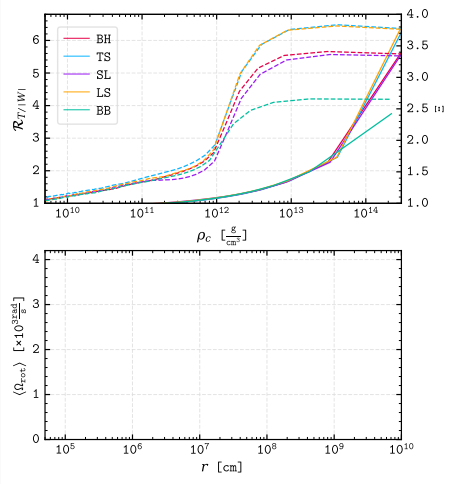
- Normalised rotational parameter of the inner core

$$\mathcal{R}_{T/|W|}(\rho_c) = \frac{T/|W|(\rho_c)}{T/|W|(t=0)};$$

- Homology deviation parameter of the inner core

$$\Xi(\rho_c) = \frac{T/|W|(\rho_c)}{T/|W|(t=0)} \frac{R(\rho_c)}{R(t=0)};$$

- Models deviate at $\sim 10^{12}\,\mathrm{g/cm^3}$;



COLLAPSE EVOLUTION

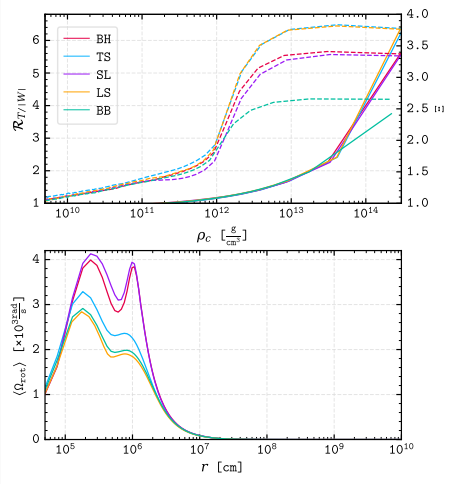
- Normalised rotational parameter of the inner core

$$\mathcal{R}_{T/|W|}(\rho_c) = \frac{T/|W|(\rho_c)}{T/|W|(t=0)};$$

- Homology deviation parameter of the inner core

$$\Xi(\rho_c) = \frac{T/|W|(\rho_c)}{T/|W|(t=0)} \frac{R(\rho_c)}{R(t=0)};$$

- Models deviate at $\sim 10^{12}\,\mathrm{g/cm^3}$;
- Different rotational profile at bounce;



COLLAPSE EVOLUTION

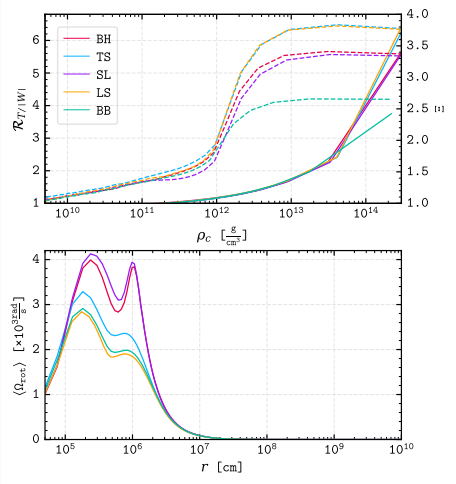
- Normalised rotational parameter of the inner core

$$\mathcal{R}_{T/|W|}(\rho_c) = \frac{T/|W|(\rho_c)}{T/|W|(t=0)};$$

- Homology deviation parameter of the inner core

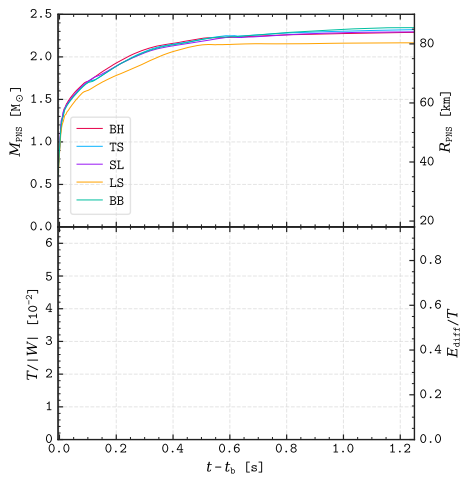
$$\Xi(\rho_c) = \frac{T/|W|(\rho_c)}{T/|W|(t=0)} \frac{R(\rho_c)}{R(t=0)};$$

- Models deviate at $\sim 10^{12}\,\mathrm{g/cm^3}$;
- Different rotational profile at bounce;
- **The EOS influences the structure of the core before core bounce.**



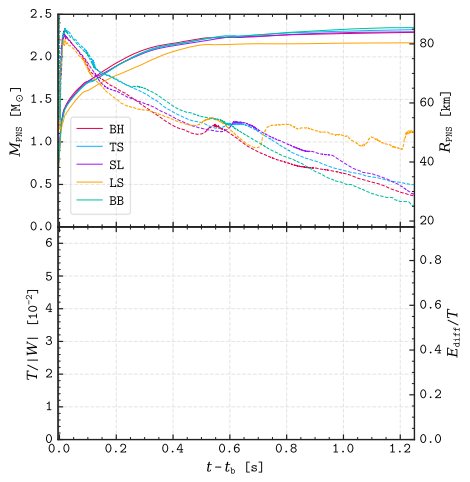
HYDRODYNAMICAL EVOLUTION OF THE PNS

- All models have a **massive PNS** ($\gtrsim 2.2\,\mathrm{M}_\odot$), with LS is $\sim 0.1\,\mathrm{M}_\odot$ lighter than the others;



HYDRODYNAMICAL EVOLUTION OF THE PNS

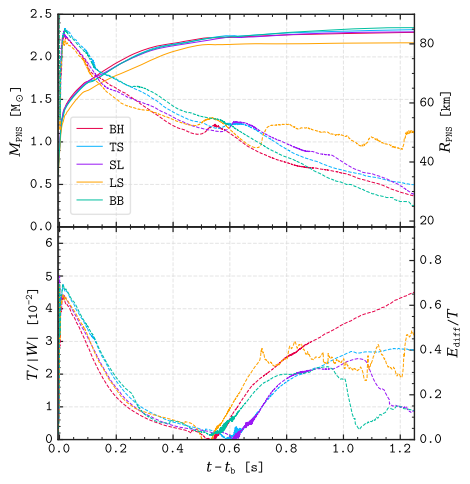
- All models have a **massive PNS** ($\gtrsim 2.2\,\mathrm{M}_\odot$), with LS is $\sim 0.1\,\mathrm{M}_\odot$ lighter than the others;
- PNS radius shows expansion at $0.5 - 0.6\,\mathrm{s}$;



HYDRODYNAMICAL EVOLUTION OF THE PNS

- All models have a **massive PNS** ($\gtrsim 2.2\,\mathrm{M}_\odot$), with LS is $\sim 0.1\,\mathrm{M}_\odot$ lighter than the others;
- PNS radius shows expansion at $0.5 - 0.6\,\mathrm{s}$;
- Differential rotation is ~ 0 at $0.5 - 0.6\,\mathrm{s}$:

$$E_{\mathrm{diff}} = T_{\mathrm{PNS}} - \frac{1}{2}\frac{J_{\mathrm{PNS}}^2}{I_{\mathrm{PNS}}};$$

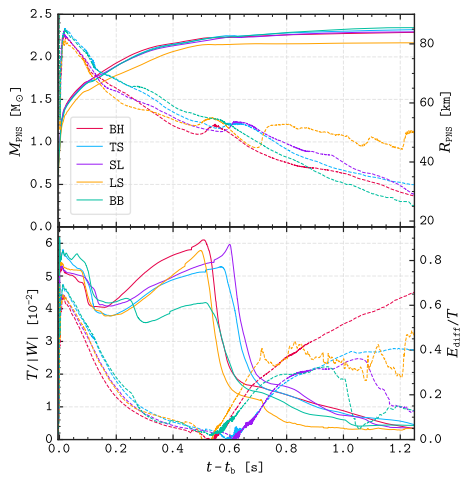


HYDRODYNAMICAL EVOLUTION OF THE PNS

- All models have a **massive PNS** ($\gtrsim 2.2\,\mathrm{M}_\odot$), with LS is $\sim 0.1\,\mathrm{M}_\odot$ lighter than the others;
- PNS radius shows expansion at $0.5 - 0.6\,\mathrm{s}$;
- Differential rotation is ~ 0 at $0.5 - 0.6\,\mathrm{s}$:

$$E_{\mathrm{diff}} = T_{\mathrm{PNS}} - \frac{1}{2}\frac{J_{\mathrm{PNS}}^2}{I_{\mathrm{PNS}}};$$

- Instabilities linked to the evolution of the $T/|W|$;

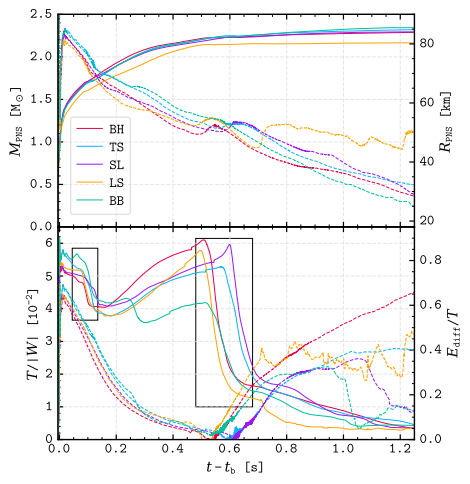


HYDRODYNAMICAL EVOLUTION OF THE PNS

- All models have a **massive PNS** ($\gtrsim 2.2\,\mathrm{M}_\odot$), with LS is $\sim 0.1\,\mathrm{M}_\odot$ lighter than the others;
- PNS radius shows expansion at $0.5 - 0.6\,\mathrm{s}$;
- Differential rotation is ~ 0 at $0.5 - 0.6\,\mathrm{s}$:

$$E_{\mathrm{diff}} = T_{\mathrm{PNS}} - \frac{1}{2}\frac{J_{\mathrm{PNS}}^2}{I_{\mathrm{PNS}}};$$

- Instabilities linked to the evolution of the $T/|W|$;
- $T/|W|$ drops significantly in two regions.

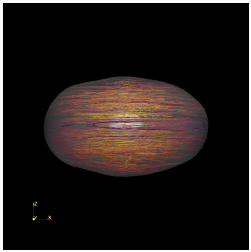


PNS ROTATION AXIS AND STRUCTURE OF THE MAGNETIC FIELD

- PNS rotation axis changes orientation over time (defined as $\hat{\mathbf{n}}_{\mathrm{PNS}} = \frac{\mathbf{J}_{\mathrm{PNS}}}{|\mathbf{J}_{\mathrm{PNS}}|}$), and the magnetic field changes accordingly;

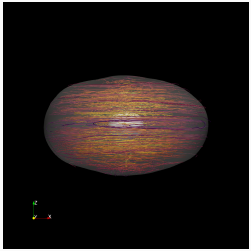
PNS ROTATION AXIS AND STRUCTURE OF THE MAGNETIC FIELD

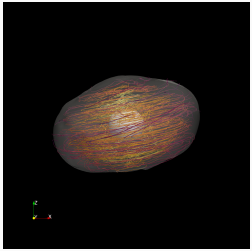
- PNS rotation axis changes orientation over time (defined as $\hat{\mathbf{n}}_{\mathrm{PNS}} = \frac{\mathbf{J}_{\mathrm{PNS}}}{|\mathbf{J}_{\mathrm{PNS}}|}$), and the magnetic field changes accordingly;
- Rotation around original rotation axis (z);



PNS ROTATION AXIS AND STRUCTURE OF THE MAGNETIC FIELD

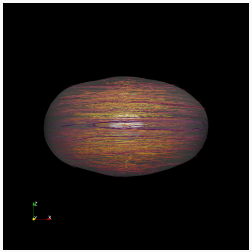
- PNS rotation axis changes orientation over time (defined as $\hat{\mathbf{n}}_{\mathrm{PNS}} = \frac{\mathbf{J}_{\mathrm{PNS}}}{|\mathbf{J}_{\mathrm{PNS}}|}$), and the magnetic field changes accordingly;
- Rotation around original rotation axis (z);
- Deviation;

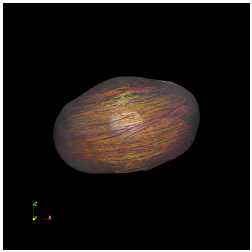


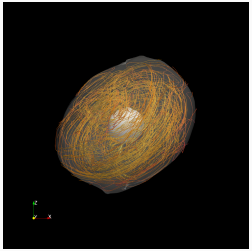


PNS ROTATION AXIS AND STRUCTURE OF THE MAGNETIC FIELD

- PNS rotation axis changes orientation over time (defined as $\hat{\mathbf{n}}_{\mathrm{PNS}} = \frac{\mathbf{J}_{\mathrm{PNS}}}{|\mathbf{J}_{\mathrm{PNS}}|}$), and the magnetic field changes accordingly;
- Rotation around original rotation axis (z);
- Deviation;
- Reaching maximum deviation;

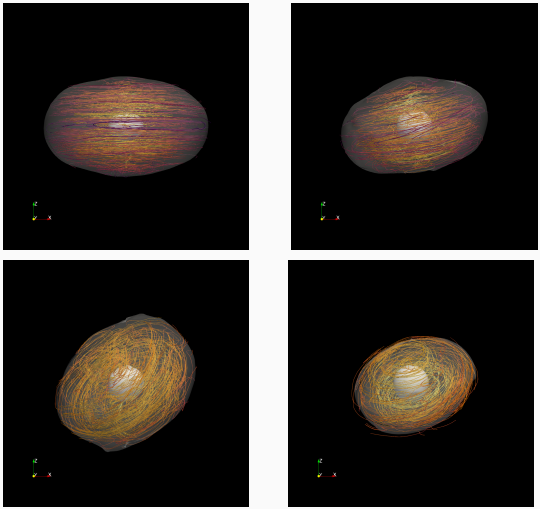






PNS ROTATION AXIS AND STRUCTURE OF THE MAGNETIC FIELD

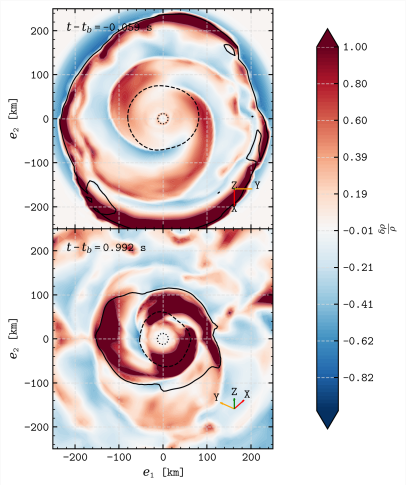
- PNS rotation axis changes orientation over time (defined as $\hat{\mathbf{n}}_{\mathrm{PNS}} = \frac{\mathbf{J}_{\mathrm{PNS}}}{|\mathbf{J}_{\mathrm{PNS}}|}$), and the magnetic field changes accordingly;
- Rotation around original rotation axis (z);
- Deviation;
- Reaching maximum deviation;
- Drift towards the original position.



LARGE SCALE STRUCTURES

- Density deviation from spherical symmetry to identify anisotropic matter structures

$$\frac{\delta\rho}{\rho} = \frac{\rho - \langle\rho\rangle_\Omega}{\langle\rho\rangle_\Omega};$$

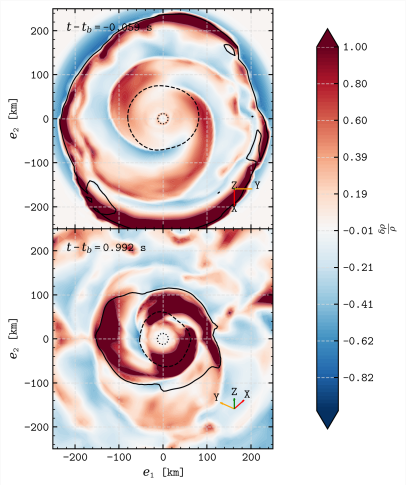


LARGE SCALE STRUCTURES

- Density deviation from spherical symmetry to identify anisotropic matter structures

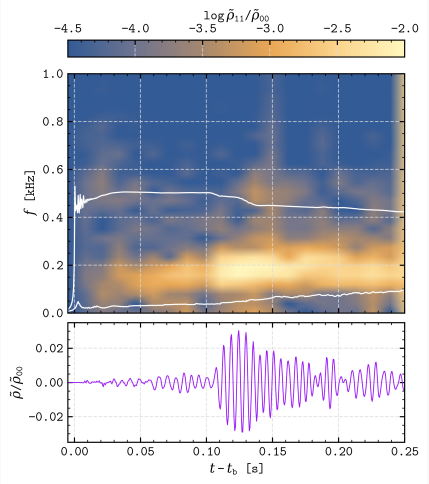
$$\frac{\delta\rho}{\rho} = \frac{\rho - \langle\rho\rangle_\Omega}{\langle\rho\rangle_\Omega};$$

- **Large scale spiral structures** develop at $\sim 0.1\,\mathrm{s}$ and $\sim 0.6\,\mathrm{s}$.



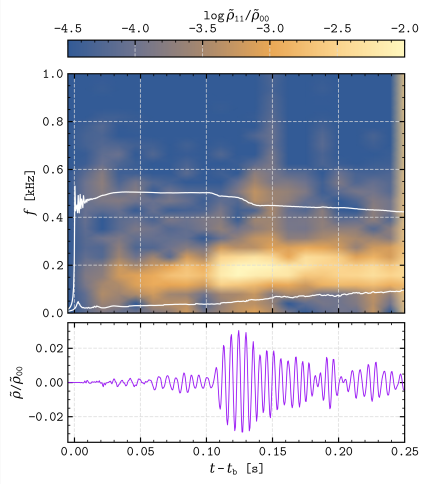
Non-axisymmetric instabilities development

- Spherical harmonics decomposition of the density, and analysis of the $\ell = m = 1$ mode;



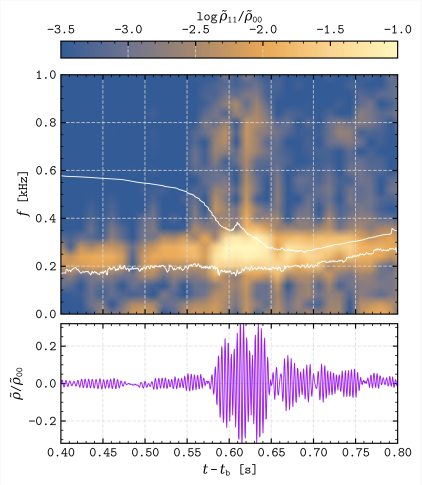
Non-axisymmetric instabilities development

- Spherical harmonics decomposition of the density, and analysis of the $\ell = m = 1$ mode;
- Low-$T/|W|$ instability (LTWI)
  - Nearly constant mode frequency;
  - Development on the equatorial plane;
  - Large amount of differential rotation available;



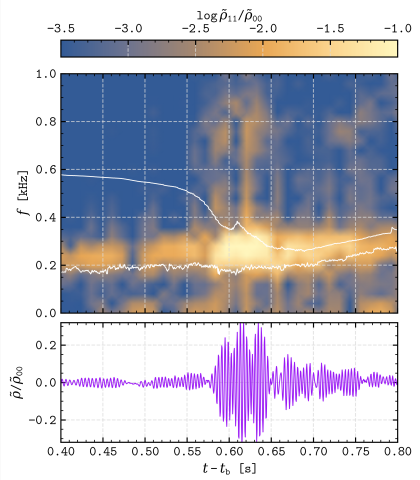
Non-axisymmetric instabilities development

- Spherical harmonics decomposition of the density, and analysis of the $\ell = m = 1$ mode;
- Low-$T/|W|$ instability (LTWI)
  - Nearly constant mode frequency;
  - Development on the equatorial plane;
  - Large amount of differential rotation available;
- Second non-axisymmetric instability (SNAI):
  - Nearly constant mode frequency;
  - Axis tilting, not restrained to the equator;
  - PNS nearly rigidly rotating;



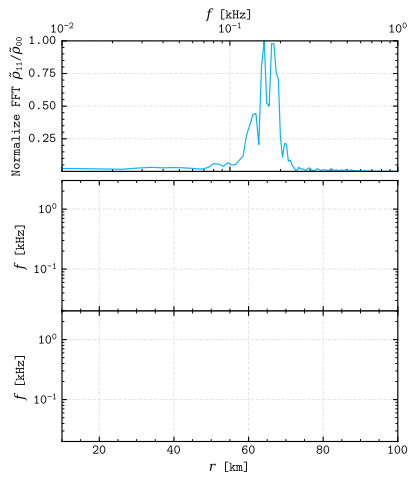
Non-axisymmetric instabilities development

- Spherical harmonics decomposition of the density, and analysis of the $\ell = m = 1$ mode;
- Low-$T/|W|$ instability (LTWI)
  - Nearly constant mode frequency;
  - Development on the equatorial plane;
  - Large amount of differential rotation available;
- Second non-axisymmetric instability (SNAI):
  - Nearly constant mode frequency;
  - Axis tilting, not restrained to the equator;
  - PNS nearly rigidly rotating;
- **Mode frequency enclosed between central and surface PNS rotation.**



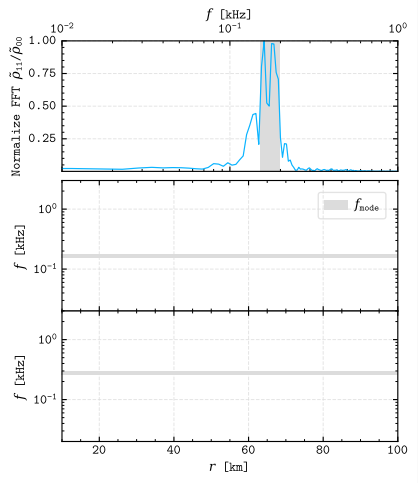
CHARACTERISATION OF THE NON-AXISYMMETRIC INSTABILITIES

- Fourier transform of the density decomposition at different radii;



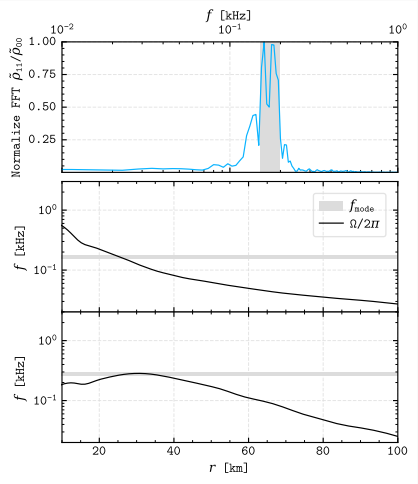
CHARACTERISATION OF THE NON-AXISYMMETRIC INSTABILITIES

- Fourier transform of the density decomposition at different radii;
- Mode frequency given by the maximum of the spectrum, and uncertainty estimated via the full width at half maximum (FWHM);



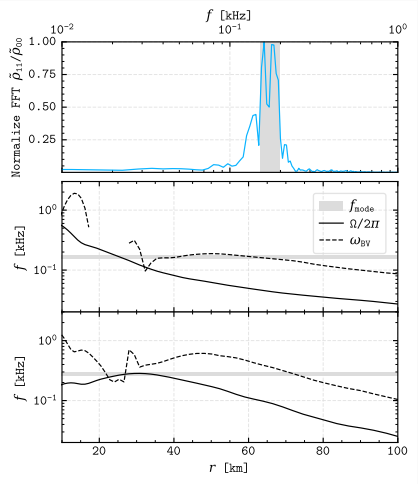
CHARACTERISATION OF THE NON-AXISYMMETRIC INSTABILITIES

- Fourier transform of the density decomposition at different radii;
- Mode frequency given by the maximum of the spectrum, and uncertainty estimated via the full width at half maximum (FWHM);
- Corotation points:
  - LTWI: far from maximum rotation (f mode Passamonti *et al* 2015);
  - SNAI: close to maximum rotation (i mode, Passamonti *et al* 2020);



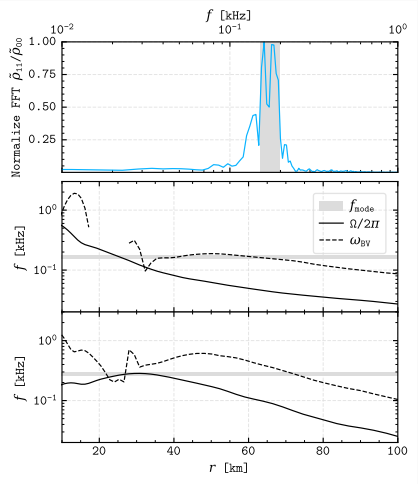
CHARACTERISATION OF THE NON-AXISYMMETRIC INSTABILITIES

- Fourier transform of the density decomposition at different radii;
- Mode frequency given by the maximum of the spectrum, and uncertainty estimated via the full width at half maximum (FWHM);
- Corotation points:
  - LTWI: far from maximum rotation (f mode Passamonti *et al* 2015);
  - SNAI: close to maximum rotation (i mode, Passamonti *et al* 2020);
- LTWI corotation point lies in a convective region;



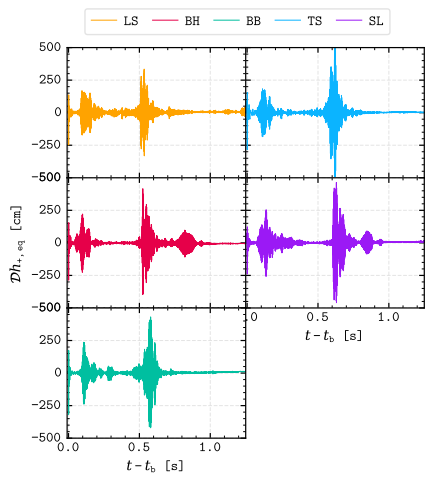
CHARACTERISATION OF THE NON-AXISYMMETRIC INSTABILITIES

- Fourier transform of the density decomposition at different radii;
- Mode frequency given by the maximum of the spectrum, and uncertainty estimated via the full width at half maximum (FWHM);
- Corotation points:
  - LTWI: far from maximum rotation (f mode Passamonti *et al* 2015);
  - SNAI: close to maximum rotation (i mode, Passamonti *et al* 2020);
- LTWI corotation point lies in a convective region;
- **Both LTWI and SNAI are corotation instabilities.**



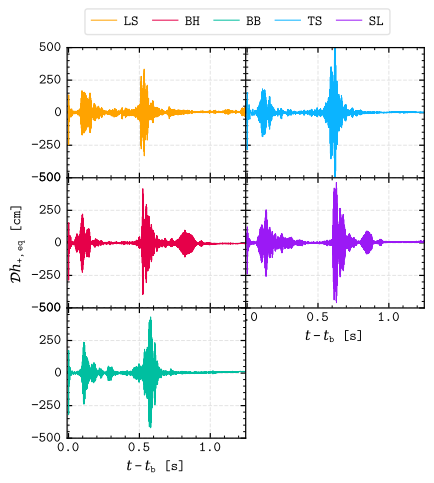
Influence of the instabilities on the GW signal

- The instabilities impact the GW emission;



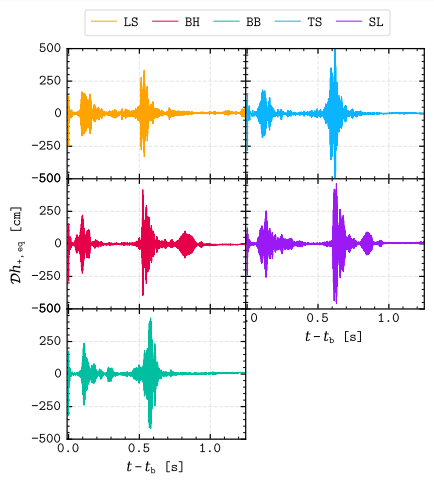
Influence of the instabilities on the GW signal

- The instabilities impact the GW emission;
- Each model develops the two instabilities;



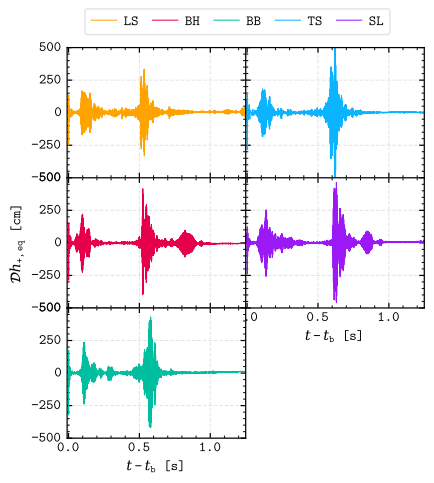
Influence of the instabilities on the GW signal

- The instabilities impact the GW emission;
- Each model develops the two instabilities;
- Different onset times;



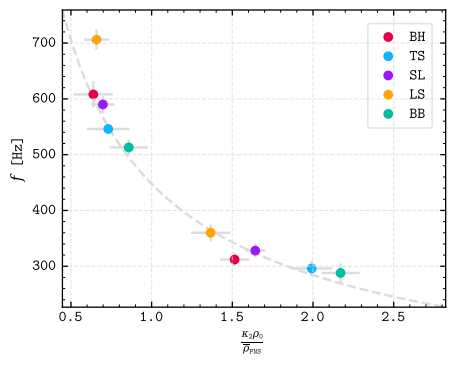
Influence of the instabilities on the GW signal

- The instabilities impact the GW emission;
- Each model develops the two instabilities;
- Different onset times;
- Different strengths.



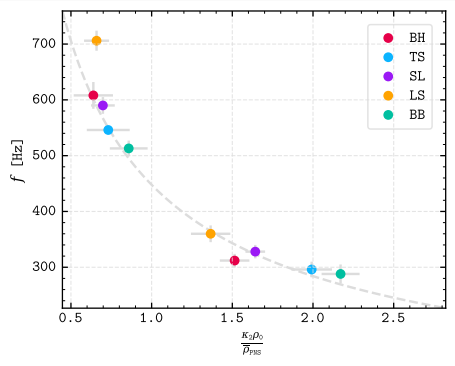
GW PEAK FREQUENCY DEPENDENCE ON THE PNS STIFFNESS

- Stiffness of the PNS estimated with the tidal Love number κ_2;



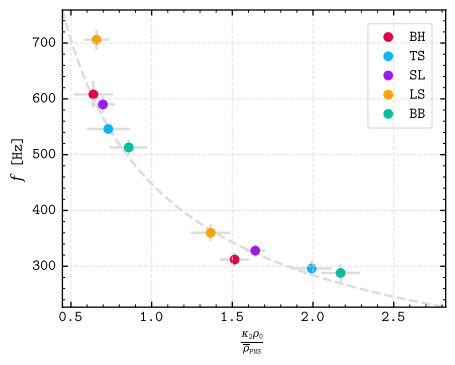
GW PEAK FREQUENCY DEPENDENCE ON THE PNS STIFFNESS

- Stiffness of the PNS estimated with the tidal Love number κ_2;
- Characteristic frequency of the GW signal estimated with the Fourier transform of the signal during which the instability is active;



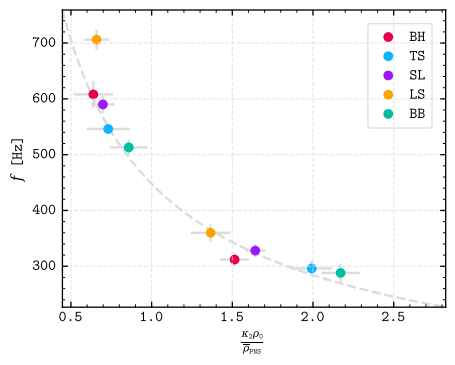
GW PEAK FREQUENCY DEPENDENCE ON THE PNS STIFFNESS

- Stiffness of the PNS estimated with the tidal Love number κ_2;
- Characteristic frequency of the GW signal estimated with the Fourier transform of the signal during which the instability is active;
- Frequency of each instability depends **linearly** on κ_2 ($R^2 \approx 0.85$);



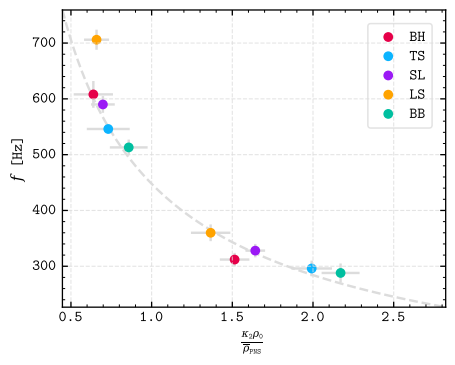
GW PEAK FREQUENCY DEPENDENCE ON THE PNS STIFFNESS

- Stiffness of the PNS estimated with the tidal Love number κ_2;
- Characteristic frequency of the GW signal estimated with the Fourier transform of the signal during which the instability is active;
- Frequency of each instability depends **linearly** on κ_2 ($R^2 \approx 0.85$);
- Together they depend on $\frac{\kappa_2 \rho_0}{\bar{\rho}_{\rm PNS}}$ ($R^2 = 0.95$);



GW PEAK FREQUENCY DEPENDENCE ON THE PNS STIFFNESS

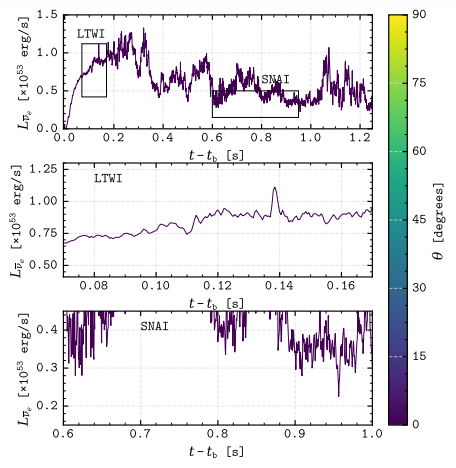
- Stiffness of the PNS estimated with the tidal Love number κ_2;
- Characteristic frequency of the GW signal estimated with the Fourier transform of the signal during which the instability is active;
- Frequency of each instability depends **linearly** on κ_2 ($R^2 \approx 0.85$);
- Together they depend on $\frac{\kappa_2 \rho_0}{\bar{\rho}_{\rm PNS}}$ ($R^2 = 0.95$);
- **Frequency of the GW signal depends on the EOS.**



Influence of the instabilities on the neutrino luminosity

- Computing the isotropic equivalent neutrino luminosity at various angles

$$L^{\mathrm{iso}}_{\nu_i}(\theta,\phi) = 4\pi r^2 F^r_{\nu_i}(r,\theta,\phi);$$

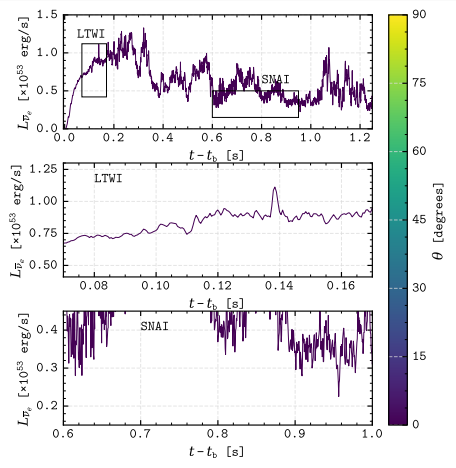


Influence of the instabilities on the neutrino luminosity

- Computing the isotropic equivalent neutrino luminosity at various angles

$$L^{\mathrm{iso}}_{\nu_i}(\theta,\phi) = 4\pi r^2 F^r_{\nu_i}(r,\theta,\phi);$$

- At the poles neutrino luminosities **do not** show imprints of the instabilities;

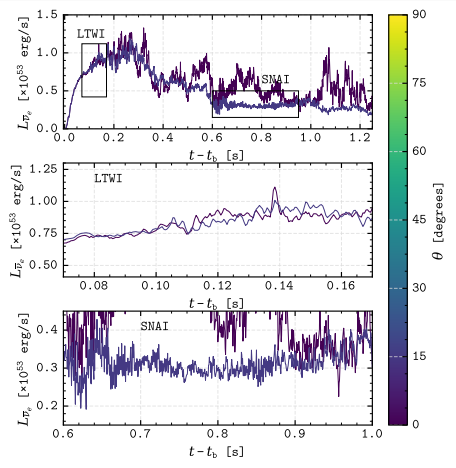


Influence of the instabilities on the neutrino luminosity

- Computing the isotropic equivalent neutrino luminosity at various angles

$$L^{\mathrm{iso}}_{\nu_i}(\theta,\phi) = 4\pi r^2 F^r_{\nu_i}(r,\theta,\phi);$$

- At the poles neutrino luminosities **do not** show imprints of the instabilities;

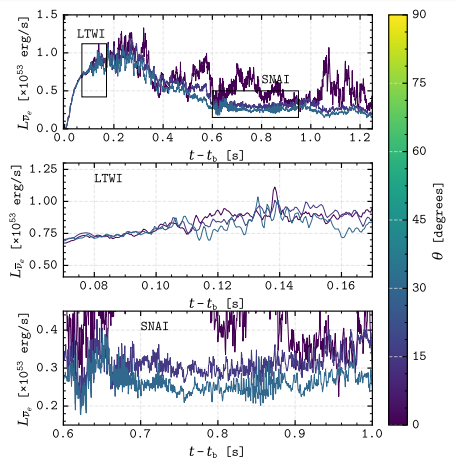


Influence of the instabilities on the neutrino luminosity

- Computing the isotropic equivalent neutrino luminosity at various angles

$$L^{\mathrm{iso}}_{\nu_i}(\theta,\phi) = 4\pi r^2 F^r_{\nu_i}(r,\theta,\phi);$$

- At the poles neutrino luminosities **do not** show imprints of the instabilities;
- Close to the equator the SNAI and LTWI **perturb the neutrino luminosity**;

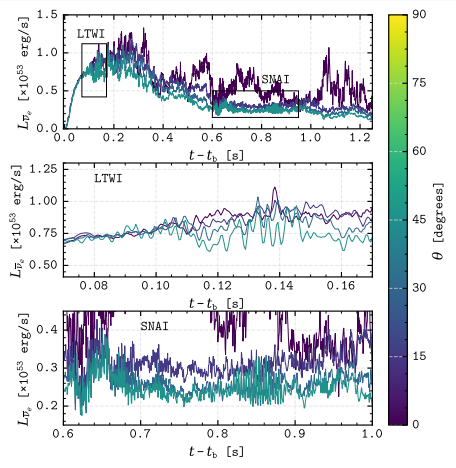


Influence of the instabilities on the neutrino luminosity

- Computing the isotropic equivalent neutrino luminosity at various angles

$$L^{\mathrm{iso}}_{\nu_i}(\theta,\phi) = 4\pi r^2 F^r_{\nu_i}(r,\theta,\phi);$$

- At the poles neutrino luminosities **do not** show imprints of the instabilities;
- Close to the equator the SNAI and LTWI **perturb the neutrino luminosity**;

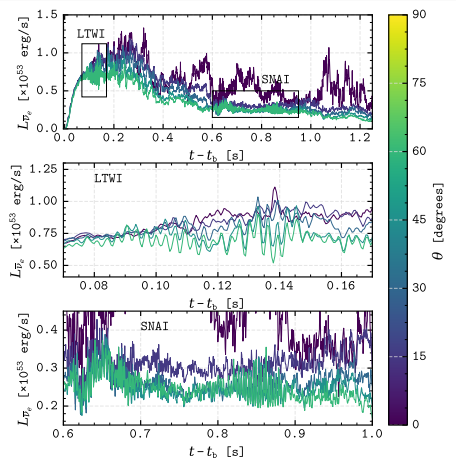


Influence of the instabilities on the neutrino luminosity

- Computing the isotropic equivalent neutrino luminosity at various angles

$$L^{\mathrm{iso}}_{\nu_i}(\theta,\phi) = 4\pi r^2 F^r_{\nu_i}(r,\theta,\phi);$$

- At the poles neutrino luminosities **do not** show imprints of the instabilities;
- Close to the equator the SNAI and LTWI **perturb the neutrino luminosity**;

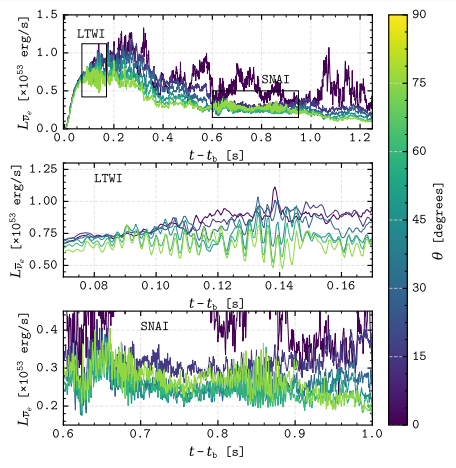


Influence of the instabilities on the neutrino luminosity

- Computing the isotropic equivalent neutrino luminosity at various angles

$$L^{\mathrm{iso}}_{\nu_i}(\theta,\phi) = 4\pi r^2 F^r_{\nu_i}(r,\theta,\phi);$$

- At the poles neutrino luminosities **do not** show imprints of the instabilities;
- Close to the equator the SNAI and LTWI **perturb the neutrino luminosity**;

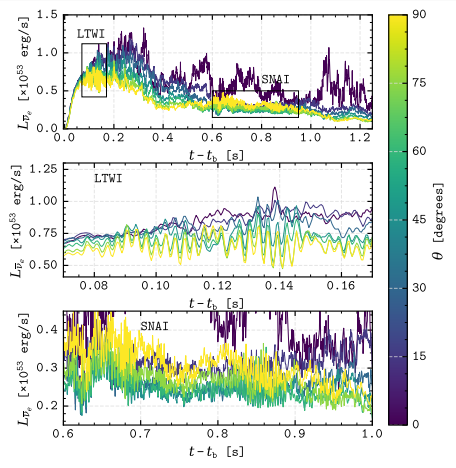


Influence of the instabilities on the neutrino luminosity

- Computing the isotropic equivalent neutrino luminosity at various angles

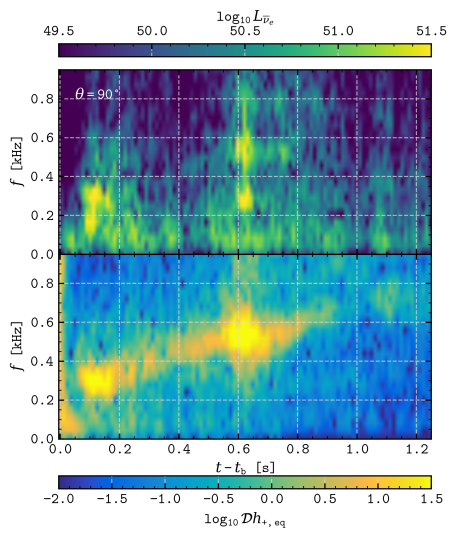
$$L^{\mathrm{iso}}_{\nu_i}(\theta,\phi) = 4\pi r^2 F^r_{\nu_i}(r,\theta,\phi);$$

- At the poles neutrino luminosities **do not** show imprints of the instabilities;
- Close to the equator the SNAI and LTWI **perturb the neutrino luminosity**;
- **SNAI** is also visible close to the **poles** due to axis tilting.



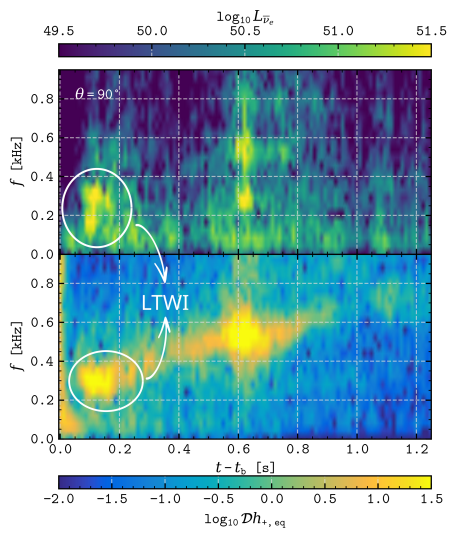
Influence of the instabilities on the neutrino and GWs spectra

- Spectrograms of the isotropic equivalent neutrino luminosity shows contribution from $(\ell, m) = (1, 1)$ and $(2, 2)$;



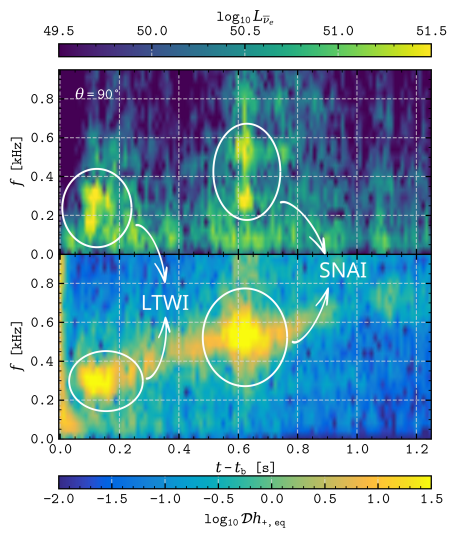
Influence of the instabilities on the neutrino and GWs spectra

- Spectrograms of the isotropic equivalent neutrino luminosity shows contribution from $(\ell, m) = (1, 1)$ and $(2, 2)$;



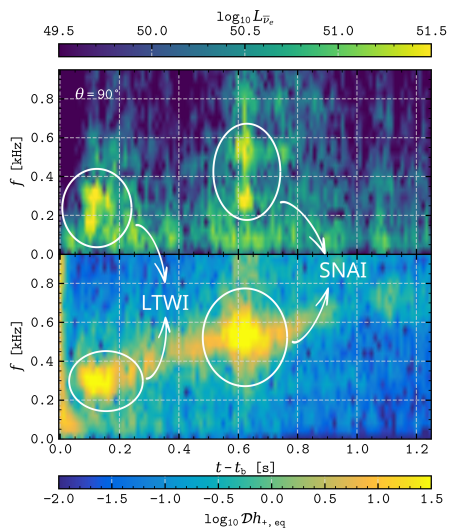
Influence of the instabilities on the neutrino and GWs spectra

- Spectrograms of the isotropic equivalent neutrino luminosity shows contribution from $(\ell, m) = (1, 1)$ and $(2, 2)$;



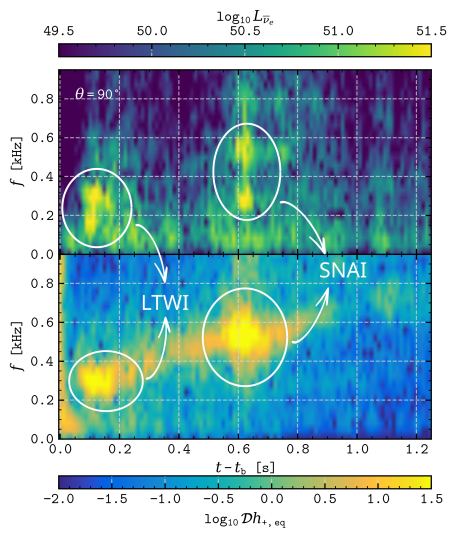
Influence of the instabilities on the neutrino and GWs spectra

- Spectrograms of the isotropic equivalent neutrino luminosity shows contribution from $(\ell, m) = (1, 1)$ and $(2, 2)$;
- Spectrograms of the GWs shows contribution **only** from $(\ell, m) = (2, 2)$;



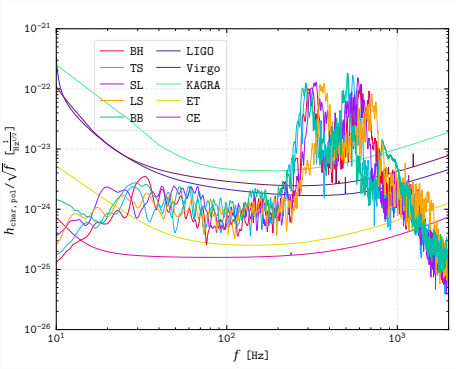
Influence of the instabilities on the neutrino and GWs spectra

- Spectrograms of the isotropic equivalent neutrino luminosity shows contribution from $(\ell, m) = (1, 1)$ and $(2, 2)$;
- Spectrograms of the GWs shows contribution **only** from $(\ell, m) = (2, 2)$;
- **Instabilities imprint a clear signature on the multimessnger emission.**



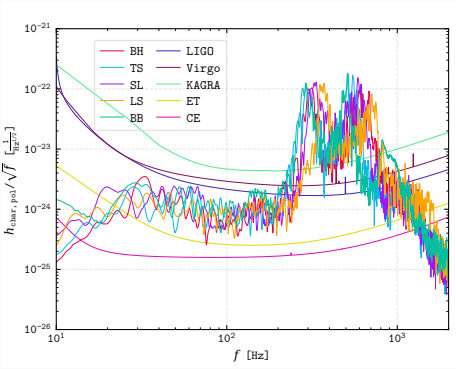
DETECTION PROSPECTS

- Detection distance estimated with an optimal signal-to-noise ratio (SNR) of 8;



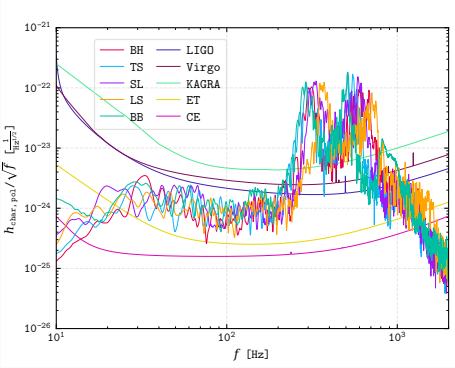
DETECTION PROSPECTS

- Detection distance estimated with an optimal signal-to-noise ratio (SNR) of 8;
- **Clear signatures** of the two instabilities at ~ 300 and $\sim 600\,\mathrm{Hz}$;



DETECTION PROSPECTS

- Detection distance estimated with an optimal signal-to-noise ratio (SNR) of 8;
- **Clear signatures** of the two instabilities at ~ 300 and $\sim 600\,\mathrm{Hz}$;
- Detection up to $3 - 4\,\mathrm{Mpc}$ (model dependent) along the polar direction in LIGO.



Conclusion

Conclusion

- The EOS impacts the evolution during collapse;

marco.cusinato@cea.fr
marco.cusinato@uv.es

Conclusion

- The EOS impacts the evolution during collapse;
- Two corotation instabilities develop forming large scale structures;

marco.cusinato@cea.fr
marco.cusinato@uv.es

Conclusion

- The EOS impacts the evolution during collapse;
- Two corotation instabilities develop forming large scale structures;
- The instabilities influence the neutrino and GW emission.

marco.cusinato@cea.fr
marco.cusinato@uv.es

Conclusion

- The EOS impacts the evolution during collapse;
- Two corotation instabilities develop forming large scale structures;
- The instabilities influence the neutrino and GW emission.



For more information on the first 250 ms of evolution.

marco.cusinato@cea.fr
marco.cusinato@uv.es

Conclusion

- The EOS impacts the evolution during collapse;
- Two corotation instabilities develop forming large scale structures;
- The instabilities influence the neutrino and GW emission.



For more information on the first 250 ms of evolution.

marco.cusinato@cea.fr
marco.cusinato@uv.es

Conclusion

- The EOS impacts the evolution during collapse;
- Two corotation instabilities develop forming large scale structures;
- The instabilities influence the neutrino and GW emission.



For more information on the first 250 ms of evolution.

marco.cusinato@cea.fr
marco.cusinato@uv.es